Temperature dependence of ion irradiation damage in the pyrochlores $La_2Zr_2O_7$ and $La_2Hf_2O_7$



2004 J. Phys.: Condens. Matter 16 8557

(http://iopscience.iop.org/0953-8984/16/47/009)

INSTITUTE OF PHYSICS PUBLISHING JOURNAL OF PHYSICS: CONDENSED MATTER

J. Phys.: Condens. Matter **16** (2004) 8557–8570 PII: S0953-8984(04)84943-9

# Temperature dependence of ion irradiation damage in the pyrochlores $La_2Zr_2O_7$ and $La_2Hf_2O_7$

**Gregory R Lumpkin**[1], **Karl R Whittle**[1,4], **Susana Rios**[1], **Katherine L Smith**[2] **and Nestor J Zaluzec**[3]

[1] Cambridge Centre for Ceramic Immobilisation, Department of Earth Sciences, University of Cambridge, Downing Street, Cambridge CB2 3EQ, UK
[2] Materials Division, Australian Nuclear Science and Technology Organisation, Private Mail Bag 1, Menai, NSW 2234, Australia
[3] Materials Science Division, Argonne National Laboratory, 9700 South Cass Avenue, Argonne, IL 60439, USA

E-mail: kwhi02@esc.cam.ac.uk

Received 14 August 2004, in final form 19 October 2004
Published 12 November 2004
Online at stacks.iop.org/JPhysCM/16/8557
doi:10.1088/0953-8984/16/47/009

**Abstract**

Synthetic samples of the pyrochlores $La_2Zr_2O_7$ and $La_2Hf_2O_7$ were irradiated *in situ* in the intermediate voltage electron microscope (IVEM-Tandem Facility) at Argonne National Laboratory using 1.0 MeV $Kr^{2+}$. Results of this study demonstrate that both pyrochlores pass through the crystalline–amorphous transformation albeit with significantly different critical amorphization dose curves. The critical dose values extrapolated to 0 K ($D_{c0}$) are $11 \pm 3 \times 10^{14}$ ions cm$^{-2}$ ($\sim$1.6 dpa) for $La_2Zr_2O_7$ and $5.5 \pm 0.7 \times 10^{14}$ ions cm$^{-2}$ ($\sim$0.9 dpa) for $La_2Hf_2O_7$. Non-linear least squares analysis of the dose–temperature curves gave values of the critical temperature ($T_c$) of $339 \pm 49$ K for $La_2Zr_2O_7$ and $563 \pm 10$ K for $La_2Hf_2O_7$. This analysis also gave values of the activation energy ($E_a$) for thermal recovery of damage of $0.02 \pm 0.01$ and $0.05 \pm 0.01$ eV for the zirconium pyrochlore and the hafnium pyrochlore, respectively. These results demonstrate that there is a major difference in the dose–temperature response dependent upon the nature of the B-site cation of these two pyrochlores. Results are discussed in terms of the pyrochlore structural parameters $r_A/r_B$ and $x$(48f) as well as the stopping powers, displacement energies, and defect energies of the materials.

[4] Author to whom any correspondence should be addressed.

  

## 1. Introduction

The pyrochlore structure type has been of considerable interest over the years due to a range of potentially useful properties such as fast-ion conductors, electrical conductivity (including superconductivity), and geometrically frustrated magnetism [1–3]. Pyrochlore is also one of the principal actinide host phases in titanate ceramics designed for the safe disposal of actinide-rich wastes, including weapons Pu [4–9]. Furthermore, the structure type is represented in natural systems where it is a major ore mineral for Nb and Ta [10–12]. The crystal chemistry and aqueous behaviour of natural pyrochlores have been extensively investigated for comparison with their synthetic counterparts in nuclear waste forms [13–18]. The aqueous durability of pyrochlore has been investigated over a range of pH values and temperatures [19–23]. These studies demonstrate that the pyrochlore structure type has excellent chemical durability, including low release rates for the lanthanide and actinide elements. Importantly, recent evidence has documented that there is no significant intrinsic effect of radiation damage on the chemical behaviour of titanium pyrochlore in pure water [24]. In parallel with the laboratory studies, studies of natural pyrochlore have largely confirmed the long-term durability of this phase in aqueous fluids [25].

A major concern for these structure types is that they will undergo a crystalline to amorphous transformation as a function of the cumulative alpha decay dose over time, which may lead to volume expansion, cracking, and reduced chemical durability (due to increased surface area). Radiation damage effects in these materials have been studied extensively using actinide doping with short-lived $^{238}$Pu ($t_{1/2}$ = 87 years) or $^{244}$Cm ($t_{1/2}$ = 18 years) [26–28], natural samples [13, 18, 29–31], and various heavy ion irradiation techniques, including irradiation of bulk samples and thin TEM specimens [32–43]. Results of the actinide doping and natural analogue work have generally shown that pyrochlores in the system $NaCa(Nb, Ta)_2O_6F$–$CaUTi_2O_7$–$Ln_2Ti_2O_7$–$Ca_2TiWO_7$ all become amorphous as a result of alpha decay processes. However, the work on natural pyrochlores has also shown that the critical amorphization dose is elevated by a factor of about two to four relative to the synthetic samples doped with short-lived actinides [25].

The ion irradiation studies, in particular those conducted on thin TEM specimens, have elucidated the effects of composition and structure on the critical amorphization dose and the critical temperature (above which the material remains crystalline). Results of these studies document the increasing radiation 'stability' as the pyrochlore structure becomes more fluorite-like [34, 36, 39]. The presence of Zr on the B-site, together with a small lanthanide cation such as Gd on the A-site, promotes fluorite-like properties and hence resistance to amorphization [39]. At least one of these studies has also shown significant differences in the dose–temperature curves for thin crystals due to the mass and energy of the incoming projectile [34]. Because Hf is one of the elements intended for use in waste form materials as a neutron absorber, the main goal of this work is to examine the crystalline–amorphous transformation and determine the critical dose of $La_2Zr_2O_7$ and $La_2Hf_2O_7$ end-member pyrochlores as a function of temperature. In this work, we use 1.0 MeV $Kr^{2+}$ ions in order to facilitate comparison with previous ion irradiation work on thin TEM specimens.

## 2. Experimental procedures

### *2.1. Synthesis*

Samples were prepared by the calcination of metal oxides. Stoichiometric amounts of lanthanum oxide (Aldrich, 99.5%), zirconium oxide (Aldrich, 99.5%), and hafnium oxide

(Alfa-Aesar, 99%) were intimately mixed in acetone slurry using a ball-mill and subsequently dried. Once dried the powders were heated at 1500 °C for 24 h, reground to an average particle size less than 10 $\mu$m, and pressed into pellets prior to calcination for a further 24 h.

### *2.2. X-ray and neutron powder diffraction*

Phase composition of the sample was confirmed by x-ray powder diffraction, using a modified Bede D1 diffractometer and weighted Cu K$\alpha$ radiation, with an angular range of 15°–80° two-theta. The resultant patterns were compared with the ICDD library of recorded patterns. Neutron powder diffraction patterns were also recorded using the C2 spectrometer at the Chalk River laboratories, Canada, using a wavelength of 0.133 nm. The neutron powder diffraction patterns were refined using the GSAS suite of software to obtain the $a$ cell parameter and the $x$(48f) oxygen positional parameter. We report only the preliminary refinements here, as the structural refinements are part of a larger study of La–Y–Hf/Zr oxide pyrochlores and will be reported in detail elsewhere.

### *2.3. Scanning electron microscopy*

All samples were checked for purity using a JEOL 6400 SEM operated at 15 kV. Inclusions, zoning, and other features were identified from a combination of secondary and backscattered electron images. Microanalyses were obtained using a Noran Voyager energy dispersive spectrometer (EDX) attached to this microscope. The instrument was operated in standardless mode; however, the sensitivity factors were calibrated for semi-quantitative analysis using a range of synthetic and natural standard materials. Spectra were usually acquired for 500 s and reduced to weight per cent oxides using a digital top hat filter to suppress the background, a library of reference spectra for multiple least squares peak fitting, and full matrix (ZAF) corrections.

### *2.4. Transmission electron microscopy*

TEM samples were prepared by crushing small fragments in methanol and collecting the suspension on holey carbon coated copper grids. Samples were characterized prior to the irradiation experiments using a JEOL 2000FXII TEM operated at 200 kV and calibrated for selected area diffraction over a range of objective lens currents using a gold film standard. The compositions of the grains were checked by EDX analysis using a Link ISIS energy dispersive spectrometer attached to the TEM. The $k$-factors required for the quantitative thin film analyses were determined from a range of synthetic and natural standard materials. Spectra were usually acquired for 600 s and processed using a digital top hat filter to suppress the background, a library of reference spectra for multiple least squares peak fitting, and a Cliff–Lorimer ratio procedure to reduce the data to weight per cent oxides. Details are given in [44].

### *2.5. Ion irradiation experiments*

Ion irradiation experiments were carried out *in situ* at the IVEM-Tandem User Facility at Argonne National Laboratory. TEM specimens were irradiated with 1.0 MeV $Kr^{2+}$ ions at room temperature using a Hitachi TEM interfaced to a NEC ion accelerator [45]. All TEM observations were carried out using an operating voltage of 300 kV; however, the electron beam was always turned off during the irradiation steps in order to avoid unnecessary complications arising from simultaneous ion–electron interactions. Ion irradiations were performed using a counting rate of 50 counts $s^{-1}$ and a flux of $3.125 \times 10^{11}$ ions $cm^{-2}$ $s^{-1}$, giving the conversion

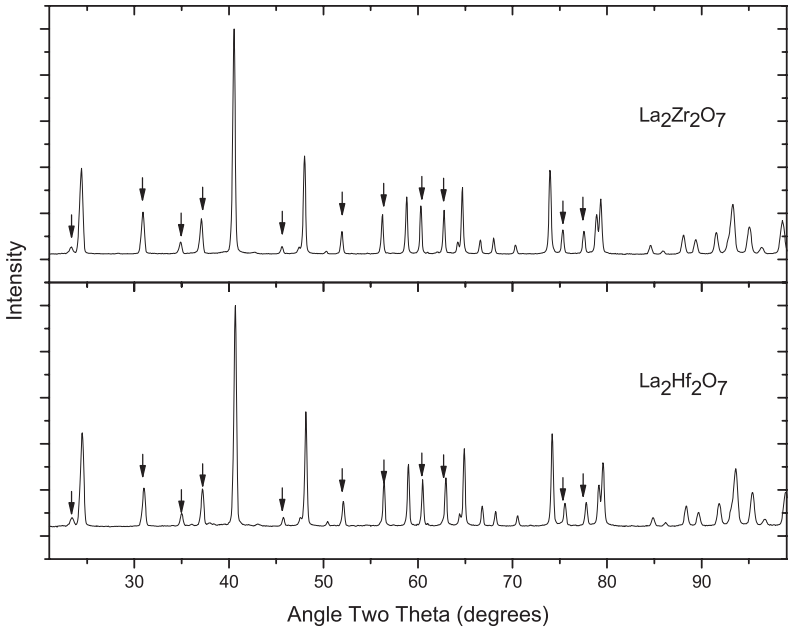


**Figure 1.** Neutron powder diffraction patterns for $La_2Zr_2O_7$ and $La_2Hf_2O_7$. Pyrochlore superlattice peaks, compared to fluorite, are indicated by arrows (below 80° two theta only). Note the similarity of the two patterns.

factor of $6.25 \times 10^9$ ions $cm^{-2}$/count. All experiments were conducted with the $x$-axis and $y$-axis tilt drives set at 0° and 13°, respectively (sample tilted toward the ion beam). The sample temperature was monitored during the room temperature irradiations and never exceeded 300 K.

Experiments were performed at temperatures down to 50 K using a sample holder equipped for liquid He cooling and up to 600 K using a different sample holder equipped for electrical heating of the sample. Temperatures were controlled to within ±1 K using these sample holders. To avoid the potential effects of ion channelling, grains were irradiated in random orientations. Each sample was irradiated using incremental dose steps and selected grains were observed using bright field imaging and selected area diffraction after each irradiation step. Using photographic negatives, the critical amorphization dose ($D_c$) was constrained to fall between the last dose increment in which Bragg diffraction spots were observed and the next increment in which only diffuse rings occur in the diffraction pattern. For each sample, we determined $D_c$ from the average of 3–6 grains (reported errors are one standard deviation on the mean value). A zirconolite reference sample with known critical amorphization dose values was irradiated in order to validate the experiments. The thickness of this sample has been checked by electron energy loss spectroscopy and is on the order of 60 nm.

## 3. Results

### *3.1. Structure and composition*

X-ray powder diffraction patterns initially indicated that the samples have the pyrochlore structure. This was confirmed by the detailed neutron powder diffraction data shown in figure 1. The two patterns are very similar and both exhibit numerous diffraction maxima arising from

**Table 1.** Average SEM-EDX (before irradiation) and TEM-EDX (after irradiation) analyses in oxide weight per cent of $La_2Zr_2O_7$ and $La_2Hf_2O_7$ samples. The respective formulae based on 7.00 oxygen atoms are given in the lower part of the table.

| | SEM-EDX results | | TEM-EDX results | |
|---|---|---|---|---|
| | $La_2Zr_2O_7$ | $La_2Hf_2O_7$ | $La_2Zr_2O_7$ | $La_2Hf_2O_7$ |
| $TiO_2$ | 0.1 | 0.1 | n.a | n.a |
| $ZrO_2$ | 41.4 | 0.0 | 41.1 | 0.4 |
| $HfO_2$ | 0.2 | 53.1 | n.a | 54.7 |
| $Y_2O_3$ | 0.0 | 0.3 | n.a | n.a |
| $La_2O_3$ | 58.3 | 46.4 | 58.9 | 45.0 |
| CaO | 0.0 | 0.1 | n.a | n.a |
| Ti | 0.01 | 0.01 | n.a | n.a |
| Zr | 1.95 | 0.00 | 1.93 | 0.02 |
| Hf | 0.01 | 1.89 | n.a | 1.94 |
| Y | 0.00 | 0.02 | n.a | n.a |
| La | 2.06 | 2.11 | 2.09 | 2.06 |
| Ca | 0.00 | 0.01 | n.a | n.a |

the pyrochlore superlattice. Using these patterns, lattice parameters of $a = 1.077\,81 \pm 0.0001$ and $1.075\,03 \pm 0.0001$ nm were determined for $La_2Zr_2O_7$ and $La_2Hf_2O_7$, respectively. These values are somewhat larger than the estimates of 1.073 74 nm for $La_2Zr_2O_7$ and 1.070 83 nm for $La_2Hf_2O_7$ which were obtained using the statistical relationship determined by Chakoumakos [46] for $A^{3+}B^{4+}$ pyrochlores. The only variable parameter in space group $Fd3m$ is the $x$(48f) oxygen coordinate (for the X site). This parameter was determined to be $0.3316 \pm 0.0001$ and $0.3310 \pm 0.0002$ for $La_2Zr_2O_7$ and $La_2Hf_2O_7$, respectively, after the first cycles of least squares refinement. These values are only slightly smaller than the estimates of 0.3333 for $La_2Zr_2O_7$ and 0.3322 for $La_2Hf_2O_7$ which were calculated from equations (1) and (2) in Chakoumakos [46], using the hard sphere ionic radii for $La^{3+}$, $Zr^{4+}$, $Hf^{4+}$, and $O^{2-}$ given by Shannon [47]. Our preliminary results for the $x$(48f) coordinate are also within the range of values given by previous investigators [47–49]. The resulting mean bond lengths are La–O = 0.255 70 nm and Zr–O = 0.209 85 nm for the zirconate, and La–O = 0.255 37 nm and Hf–O = 0.209 04 nm for the hafnate. These values represent differences of 0.13% for the La–O bonds and 0.39% for the Zr–O and Hf–O bonds in the two samples.

SEM-EDX results indicate that both samples are chemically homogeneous and close to the nominal starting compositions. Backscattered electron images reveal little, if any, variation in contrast between these samples. Furthermore, EDX analyses of individual grains show only minor variations in composition. Average EDX analyses of each sample are given in table 1. The chemical formulae of the two pyrochlores are also shown, based on the normalization to 7.00 oxygen atoms. Average compositions of the two samples are $La_{2.06}Zr_{1.95}Ti_{0.01}Hf_{0.01}O_7$ and $La_{2.11}Y_{0.02}Ca_{0.01}Ti_{0.01}Hf_{1.89}O_7$. Considering the analytical fitting errors of $\pm 0.05$ atoms/fu for La, Zr, and Hf, together with additional smaller errors of $\pm 0.01$–0.02 atoms/fu due to counting statistics, the analyses are reasonably close to the ideal $A_2B_2O_7$ stoichiometry of pyrochlore (e.g., within $\pm 2$ standard deviations). In addition to the SEM-EDX results reported above, we performed *ex situ* TEM-EDX thin film analyses of the grains after the irradiation experiments were completed. Results of these analyses, based on 7.00 oxygen atoms per formula unit, give average compositions of $La_{2.09}Zr_{1.93}O_7$ and $La_{2.06}Zr_{0.02}Hf_{1.94}O_7$ for the two samples. These results are within error of the SEM-EDX analyses.

**Table 2.** Average critical amorphization dose values (and errors) for $La_2Zr_2O_7$ and $La_2Hf_2O_7$ samples irradiated with 1.0 MeV $Kr^{2+}$ ions. All dose values are given in units of $10^{14}$ ions $cm^{-2}$. Errors represent one standard deviation on the mean of several measurements at each temperature.

| | $La_2Zr_2O_7$ | | $La_2Hf_2O_7$ | |
|---|---|---|---|---|
| $T$ (K) | $D_c$ | Error | $D_c$ | Error |
| 50 | 11.6 | 2.6 | 5.5 | 0.8 |
| 150 | 20.0 | 3.6 | 5.9 | 1.2 |
| 200 | 38.8 | 7.5 | — | — |
| 250 | 59.4 | — | 7.6 | 1.0 |
| 350 | — | — | 12.2 | 1.0 |
| 500 | — | — | 47.0 | — |

### *3.2. Ion irradiation damage*

In this and previous studies, we observed that, for temperatures well below the critical temperature, increasing dose resulted in continuous reductions in the number and intensity of Bragg reflections coupled with the appearance and increasing intensity of diffuse rings in selected area diffraction patterns. Variations in the individual critical dose values may be as high as 10–25% for samples of the same composition. At temperatures closer to the critical temperature, when most of the Bragg reflections had disappeared, further increases in dose did not always lead to a further decrease in the intensity of Bragg reflections, and in some cases the number and intensity of Bragg reflections actually increased. By measuring multiple grains of the same sample, we find that the critical dose values may vary by more than 50% in the vicinity of the critical temperature, leading to additional uncertainty in subsequent data analyses. Note that we have not attempted to analyse changes in the Bragg beam intensities in detail due to the strong dynamic scattering of electrons in these high atomic number materials. For elements with high electron scattering cross-sections like Zr, La, and Hf in the pyrochlore lattice, we have calculated that the elastic mean free path is on the order of 17–70 nm for accelerating voltages of 100–300 kV. This means that, for sample thicknesses up to 100–200 nm, the electron beam intensities are dominated by multiple scattering and no longer approximate to the kinematic, single-scattering case for selected area diffraction.

We found that both pyrochlores can be rendered amorphous by irradiation with 1.0 MeV $Kr^{2+}$ ions. Results for $La_2Zr_2O_7$ irradiated at 50, 150, 200, and 250 K are listed in table 2. The critical amorphization dose ($D_c$) of $La_2Zr_2O_7$ as determined by electron diffraction increases from $11.6 \times 10^{14}$ ions $cm^{-2}$ to $59.4 \times 10^{14}$ ions $cm^{-2}$ over this temperature range. However, at 250 K only one of the five monitored grains reached the fully amorphous state, so the critical dose value given for this temperature is a minimum value. Furthermore, the single grain that became amorphous recrystallized at the highest dose of $79.2 \times 10^{14}$ ions $cm^{-2}$. Of the four grains that did not become amorphous at 250 K, TEM observations clearly show that they all exhibit diffuse rings in the electron diffraction patterns which increase in intensity with ion dose. At the highest damage state, only two Bragg diffraction spots remain in the pattern, indicating an approach toward complete amorphization. This is consistent with bright field images of the four crystals, showing lower contrast and rounding of initially angular morphological features. However, upon further irradiation to the highest dose level, these four crystals showed little further change on irradiation, suggesting that the critical temperature ($T_c$) of $La_2Zr_2O_7$ is greater than, but probably close to, 250 K.

Results for $La_2Hf_2O_7$ irradiated at 50, 150, 250, 350, and 500 K are listed in table 2. Over this temperature range, the $D_c$ values of $La_2Hf_2O_7$ range from $5.5 \times 10^{14}$ ions $cm^{-2}$

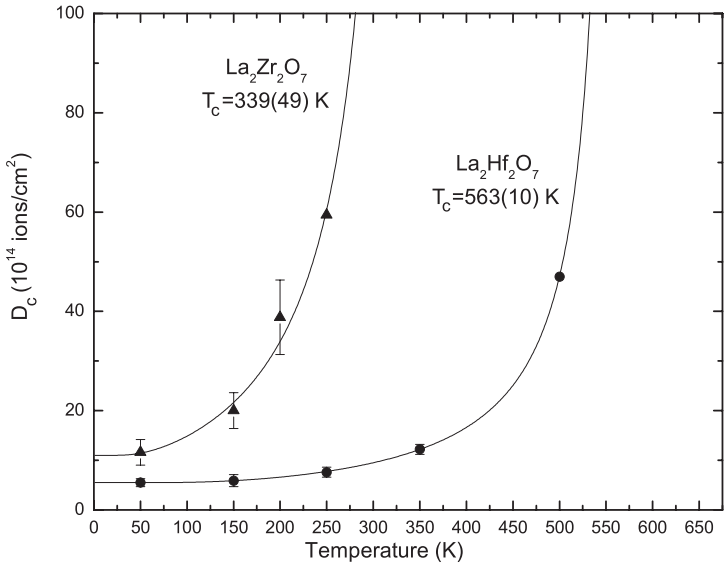


**Figure 2.** Plot of the critical amorphization dose, $D_c$, versus temperature for $La_2Zr_2O_7$ and $La_2Hf_2O_7$. The curves were obtained by non-linear least squares fitting of equation (1) to the data.

to $47 \times 10^{14}$ ions cm$^{-2}$. At 500 K two of the six grains that we examined tilted away from their original orientations far enough to be considered unusable. None of the remaining four grains reached the fully amorphous state at 500 K, therefore the dose value quoted above for this temperature represents a minimum value for the critical dose. These grains behaved in a similar fashion to the zirconate sample, showing diffuse rings in the electron diffraction pattern and a decreasing number of Bragg spots until only two remained at the highest level of damage. At this level of damage, the crystals also exhibit lower contrast and rounding of angular features. Nevertheless, upon irradiation to the highest dose level all four grains showed little further change in the diffraction pattern, with minor variations in the number and intensity of the Bragg beams. Based upon these results, the critical temperature ($T_c$) of $La_2Hf_2O_7$ is probably close to 500 K.

### *3.3. Annealing kinetics*

Weber, Wang, Meldrum, and co-workers have developed and used several expressions describing the kinetics of radiation damage production and annealing in crystalline solids [37, 40, 50]. The *in situ* TEM data are commonly analysed using the equation given below [37]:

$$D_c = D_{c0}/(1 - e[(E_a/k)(1/T_c - 1/T)]). \tag{1}$$

In this equation, $D_c$ is the critical amorphization dose, $D_{c0}$ is the critical dose at 0 K, $E_a$ is the activation energy for recovery of radiation damage, $k$ is the Boltzmann constant, $T_c$ is the critical temperature above which the specimen remains crystalline, and $T$ is the temperature. The critical dose extrapolated to 0 K ($D_{c0}$), critical temperature ($T_c$), and activation energy ($E_a$) for thermal recovery of damage were determined by non-linear least squares refinement of the data listed in table 2. Allowing all three parameters to vary, the results of these refinements are plotted in figure 2 and gave values of $D_{c0} = 11 \pm 3 \times 10^{14}$ ions cm$^{-2}$ ($\sim$1.6 dpa), $T_c = 339 \pm 49$ K, and $E_a = 0.02 \pm 0.01$ eV for $La_2Zr_2O_7$. Similarly, we found values of

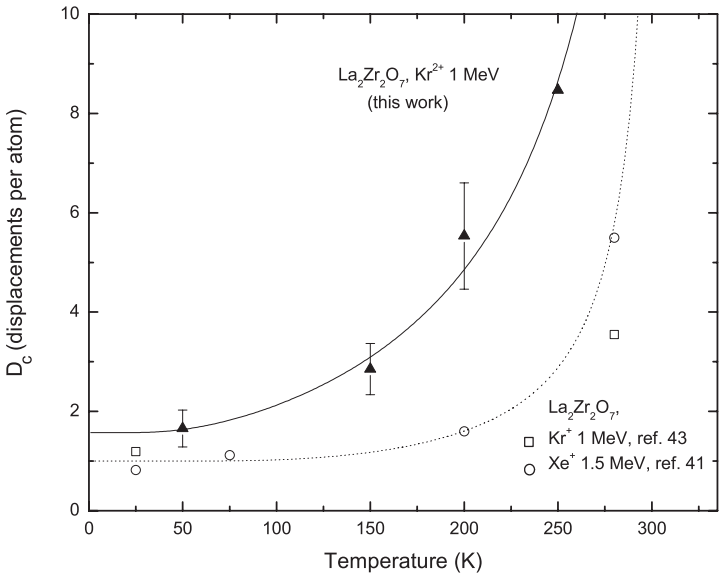


**Figure 3.** Plot of the critical amorphization dose in displacements per atom, dpa, versus temperature for $La_2Zr_2O_7$. This figure compares the behaviour during irradiation with 1.0 MeV $Kr^{2+}$ (this study, solid triangles) and 1.5 MeV $Xe^+$ ions (open circles, see [41]). The open squares refer to additional data points obtained using 1.0 MeV $Kr^+$ ions (from [43]).

$D_{c0} = 5.5 \pm 0.7 \times 10^{14}$ ions cm$^{-2}$ (∼0.9 dpa), $T_c = 563 \pm 10$ K, and $E_a = 0.05 \pm 0.01$ eV for $La_2Hf_2O_7$. The dpa values used were calculated using SRIM version 2000, displacement energies ($E_d$) of 50 eV for all atoms, and densities of 6.05 and 7.90 g cm$^{-3}$ for $La_2Zr_2O_7$ and $La_2Hf_2O_7$, respectively, and the maximum in displaced atoms versus depth.

At this point, we briefly address the results of previous published ion irradiation results for $La_2Zr_2O_7$. Lian *et al* [41] recently reported dose–temperature data obtained with 1.5 MeV $Xe^+$ ions, using the HVEM-Tandem Facility at ANL (now decommissioned). Unfortunately, the raw experimental dose values are not given in this paper, having been converted to displacements per atom (dpa). Lian *et al* [41] reported a similar critical temperature of about 310 K and activation energy for thermal annealing of 0.04 eV. No errors were given for these values. We have recalculated our dose values to units of dpa using SRIM in order to compare the two data sets (see details above). The results are shown in figure 3, where the effects of irradiation with the heavier and more energetic Xe ions are seen to give lower critical dose values, especially at the higher temperatures. In order to convert from flux, in ions cm$^{-2}$, to displacements per atom, dpa, we use SRIM to calculate damage as a function of penetration, take the peak of this curve, multiply it by the flux, and divide it by the number of atoms/nm$^3$ [51]. Comparison of the dpa values in this paper with those obtained by previous authors is difficult as it is not always clear what variables were input to SRIM and whether peak or averaged damage values were used in calculations.

We fitted the data of Lian *et al* [41] with equation (1) and determined values of $D_{c0} = 1.0$ dpa, $T_c = 336 \pm 16$ K, and $E_a = 0.04 \pm 0.01$ eV for $La_2Zr_2O_7$ irradiated with 1.5 MeV $Xe^+$ ions. These results are very similar to the results of this work, except for the lower intercept value for the dpa at 0 K. Note that, even though the non-linear least squares fit is good, the value of $T_c$ is probably not well constrained as $D_c$ exhibits little variation as a function of temperature (e.g., minimal upward curvature, a typical problem in these experiments).

When comparing the results obtained for $La_2Zr_2O_7$ in our present work (1 MeV $Kr^{2+}$) with those reported in the literature (1.5 MeV $Xe^+$, [41]), the difference can clearly be explained. The lower $D_{c0}$ reported in the literature is due to the fact the Xe creates a larger number of atomic displacements, as shown by SRIM calculations ($1 \times 10^{-8}$ atoms/ion/cm for Kr versus $1.8 \times 10^{-8}$ atoms/ion/cm for Xe), and therefore is easier to amorphize at 0 K. For the same reason, since more damage is created in the case of Xe ions, the curve in figure 3 as a function of temperature shows a slower recovery, and thus a different shape. $T_c$, however, should remain similar for both irradiation conditions if we assume that Kr 1 MeV and Xe 1.5 MeV introduce the same type of structural damage.

## 4. Discussion

In order to pursue an explanation for the observed difference in the dose–temperature response of our two samples, several experimental factors and intrinsic material properties must be considered. The potential experimental factors include systematic differences in crystallographic orientation and sample thickness. The orientation of the sample holder was unchanged during the irradiations, leaving only the crystallographic orientations of the individual crystals as a variable parameter. This does not appear to have a major effect on the determination of $D_c$ as long as one or more reasonably intense low angle diffracted beams are present. In fact, we have tested this method over a period of several years using the same synthetic zirconolite sample as a reference material. Repeated analysis of this sample shows that $D_c$ is reproduced *for different crystallographic orientations* to within $\pm 10\%$ at room temperature. Crystal thickness, on the other hand, plays a major role in determining the number of atomic displacements per ion in this type of experiment and, in general, has not been considered quantitatively due to the difficulty of measuring sample thickness in the TEM. We illustrate the potential effects of specimen thickness in figure 4. The SRIM simulations for $La_2Zr_2O_7$ indicate that, over the thickness range of 40–80 nm, for example, the number of displacements per ion may vary by a factor of about 2.5. This thickness range represents variation by a factor of 2 about the measured thickness value of 60 nm for our zirconolite reference sample. A similar conclusion may be drawn from the simulations for $La_2Hf_2O_7$. However, most of the crystals we monitored are highly transparent to 300 keV electrons, exhibit similar diffracted and transmitted beam intensities, and have similar contrast following amorphization. Thus the crystal thickness is probably similar from grain to grain and we expect differences in thickness to be averaged out according to the experimental procedures used in this study.

Intrinsic material properties include details of the chemical composition, crystal structure, and other factors such as the stopping power for Kr ions (thus the number of displacements per ion) and the displacement energies of the atoms. We have already shown from the SEM-EDX and TEM-EDX analyses that both samples are reasonably homogeneous and close to nominal stoichiometry. The minor differences observed from grain to grain should not have a significant influence on the results and will be averaged out using our experimental procedures. SRIM simulations discussed above also indicate a systematic difference in the number of displacements per ion, $N_d$, of about 20–25% for the two pyrochlores, with the hafnate giving the larger values (figure 4). Since the atomic density of the two materials is very similar, this difference may be due to a difference in the stopping power. At the initial ion energy of 1.0 MeV the nuclear stopping power is 1361 eV $nm^{-1}$ for the hafnate and 1250 eV $nm^{-1}$ for the zirconate. Furthermore, the electronic to nuclear stopping power ratio is systematically lower in the case of the hafnate, providing a plausible explanation for the difference in the number of displacements. Although this result does not account for $D_{c0}$ being lower by a factor of two in the hafnate pyrochlore, it is qualitatively in the right direction.

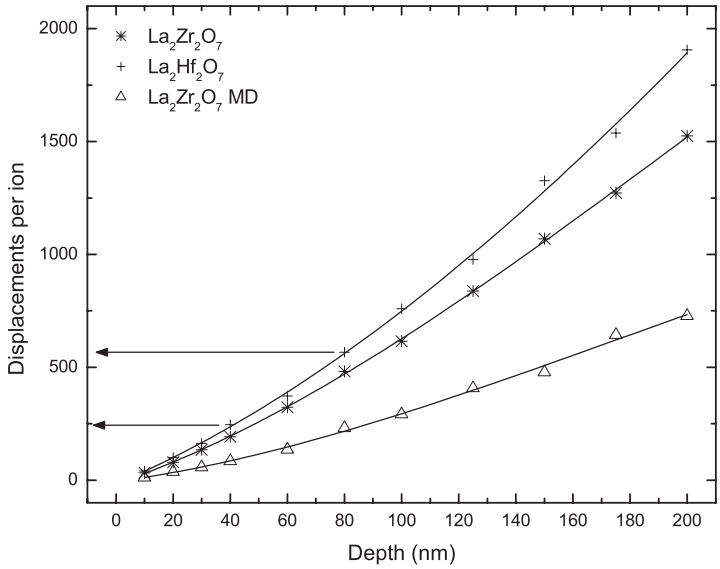


**Figure 4.** Number of displacements per ion as a function of thickness calculated for $La_2Zr_2O_7$ and $La_2Hf_2O_7$ using SRIM 2000 assuming $E_d = 50$ eV for La, Zr, Hf, and O. The arrows give an example of the potential variation in the number of displaced atoms if thickness varies from 40 to 80 nm. The lower curve illustrates the potential effect of higher cation displacement energies for $La_2Zr_2O_7$ (see [55]).

The threshold displacement energy, $E_d$, required to permanently knock an atom out of its normal lattice site has been of interest in recent years and plays a major role in determining the displacements per ion [52]. Cooper and co-workers have recently measured new $E_d$ values for oxygen in several perovskite, pyrochlore, and zirconolite compositions [53, 54]. All of the values fall within the range of 45–53 eV. Since the lattice is dominated by oxygen, large differences in the cation displacement energies would be required in order to explain even small differences in $D_{c0}$, for example. A recent trend has seen the calculation of displacement energies from molecular dynamics (MD) simulations. Calculations for zirconolite gave $E_d$ values of 25 eV for Ca, 48 eV for Zr, 43 eV for Ti, and 15 eV for O [55], the latter result being much lower than the experimental value of $45 \pm 4$ eV [54]. In another MD study, Chartier *et al* [56] reported average $E_d$ values of 153 eV for La, 188 eV for Zr, and 42 for O in $La_2Zr_2O_7$. The result for oxygen is close to the experimental value of $47 \pm 5$ eV [55]. Cation displacement energies, on the other hand, are clearly much larger than any previously reported by experiment or calculation. Figure 4 also illustrates the potential effect of the large cation displacement energies in $La_2Zr_2O_7$. Provided that the $E_d$ calculations [56] are accurate, the calculated displacements are reduced by about 50% relative to those obtained assuming $E_d = 50$ eV for cations and oxygen. Thus, the cation displacement energies of $La_2Zr_2O_7$ must be higher by a factor of three to four in order to account for the factor of two difference in the $D_{c0}$ values of our two samples. Based upon the experimental results of Cooper *et al* [54] the structural similarity of pyrochlore and zirconolite, and the fact that so many of the irradiated pyrochlores have similar $D_{c0}$ values, it seems unlikely that there will be such large differences in the threshold displacement energies.

Neutron diffraction results show that $La_2Zr_2O_7$ and $La_2Hf_2O_7$ both possess the pyrochlore structure with $x$(48f) values of approximately 0.331–0.332. However, as we have seen in

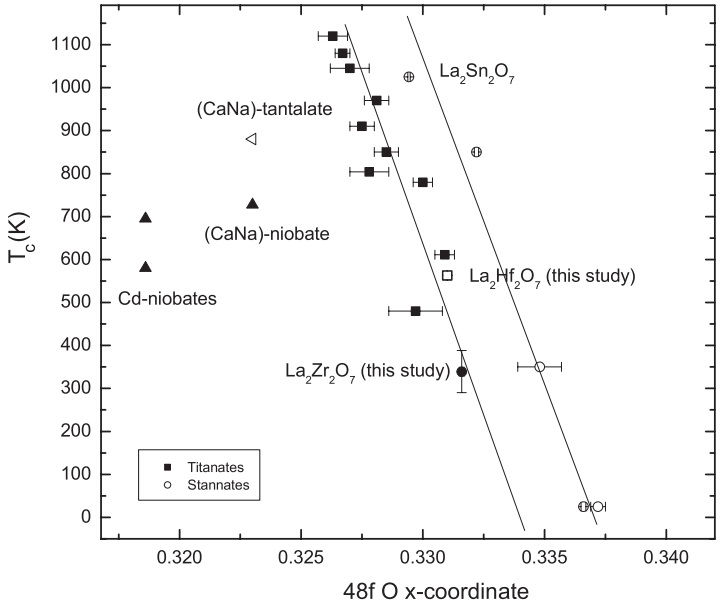


**Figure 5.** Plot of the critical temperature, $T_c$, versus the $x$(48f) oxygen coordinate for Ti, Zr, Hf, Sn, Nb, and Ta pyrochlores (from this work and [56–58, 60, 61]; some values of the oxygen coordinate are from [46] and unpublished data of the authors). The data reveal distinct trends for the Ti and Sn pyrochlores, possibly due to differences in bonding.

previous studies [41], there is a clear trend toward increased 'radiation resistance' as the structure becomes more fluorite-like (e.g., lower A/B cation ratios and a shift in the 48f oxygen coordinate toward 0.375). Based on the ionic radii of Zr (0.072 nm) and Hf (0.071 nm) in octahedral coordination [47], we expect the hafnate ($r_A/r_B = 1.634$) to have decreased radiation resistance relative to the zirconate ($r_A/r_B = 1.611$). In a detailed study of titanate pyrochlores, Lian and co-workers [57] examined variations in the critical temperature as a function of the cation radius ratio. They show that $T_c$ is positively correlated with the radius ratio over the range of $r_A/r_B = 1.61$–$1.78$; however, the overall trend appears to be non-linear with a number of minor discontinuities. Based upon the titanate data [57], the small difference in $r_A/r_B$ (0.023) produces an expected difference in the critical temperature of approximately 80 K for our samples. A similar difference is predicted using the range of observed $x$(48f) values, about a factor of three smaller than the observed difference of 224 K.

To investigate this problem further, we illustrate the relationships between $x$(48f) and $T_c$ in figure 5. Here we observe clear and separate trends in the data for the III–IV pyrochlores with Ti and Sn on the B-site. These trends may in fact be non-linear and we show them as straight lines for illustration only. The two trends may reflect differences in the bonding between Ti and Sn, as indicated by their Pauling electronegativity values of 1.54 and 1.96, respectively. Lian *et al* [58, 59] have suggested increased covalency of Sn as an explanation for the radiation response of certain stannate pyrochlores. Their conclusion was based upon the bond valence calculations of Kennedy *et al* [60]. However, a detailed analysis of the bond valence sums shows that Sn actually becomes more ionic and the lanthanides become more covalent with increasing $x$(48f) in this series. This underscores the importance of considering the bonding of all atoms in the structure. Included for comparison in figure 5 are the available data for $Cd_2Nb_2O_7$ irradiated with 280 keV Ne and 1.2 MeV Xe ions [61] and the two natural pyrochlores $NaCaNb_2O_6F$

and $NaCaTa_2O_6F$ [62]. The electronegativities of Nb and Ta are 1.6 and 1.5, respectively, and therefore similar to Ti. For the two natural pyrochlores, however, the average electronegativity of the two A-site cations (0.965) together with the high electronegativity of F (3.98) leads to increased ionicity. On further analysis, the average electronegativity difference between anions and cations decreases from the two natural pyrochlores (2.3–2.2) to the titanate series (2.1–2.0) to the stannate series (1.9–1.8). Although $Cd_2Nb_2O_7$ does not fit this pattern, the results suggest that pyrochlore systematics may be understood from further studies of the structural and bonding trends.

Finally, our $La_2Zr_2O_7$ and $La_2Hf_2O_7$ samples plot near the lower part of the titanate trend of figure 5. The individual B-site cations Zr and Hf have similar electronegativities of 1.33 and 1.30, respectively, and the average electronegativity difference for the two samples $(2.24-2.22)$ falls between the titanates and the two natural pyrochlores. One may see the effect of changing the B-site cation from the steep trend upon going from $La_2Sn_2O_7$ to $La_2Hf_2O_7$ to $La_2Zr_2O_7$ in figure 5. For III–IV pyrochlores with relatively large B-site cations in the range of 0.069–0.072 nm, large changes in the critical temperature result from small changes in structural parameters. Increasing ionicity of the B-site cation may play a major role here; however, other parameters such as defect energies (cation antisite or anion Frenkel or both) need to be considered [63, 64]. We note that calculated defect formation energies are, in general, positively correlated with the cation radius ratio, therefore they will decrease toward the lower left corner of figure 5. Ultimately, it appears that low cation defect migration energies promote radiation damage recovery in these pyrochlore thin films through increased defect migration and recombination. This suggestion is supported by close examination of the results presented by Chartier *et al* [56]. Molecular dynamic simulations of low energy alpha-recoil cascades show that at 350 K 90% of the displaced cations and oxygens within the cascade recover to either their equivalent or anti-site positions. The defect formation of the cation anti-site, i.e. La can reside on a Zr/Hf site and vice versa, is only $\sim$2 eV. This process correlates with increased ionic conductivity (by up to three orders of magnitude) as the $x$(48f) oxygen coordinate shifts from pyrochlore to fluorite-like values [1].

In conclusion, we have demonstrated that the effect of substitutions on the B-site, for ionic radii in the vicinity of 0.069–0.072 nm, has a much greater effect on the critical temperature than predicted from the established titanate trend. We will report on the form of the $T_c$ surface in $r_A$–$r_B$ space for III–IV pyrochlores in forthcoming work. The results of this study imply that the addition of Hf, in the role of a neutron absorber (100 b), will tend to lower the $D_{c0}$ value and raise the $T_c$ value of the proposed zirconate pyrochlore waste form. This effect will vary, of course, depending on the baseline composition of the waste form and the combined effects of the actinides and any other elemental impurities in the waste stream. The above conclusions are, of course, based entirely upon the results of 1.0 MeV Kr ion irradiation of thin TEM specimens and we have already seen how the separate dose–temperature curves for lanthanide titanate pyrochlores collapse to a single response curve when irradiated with 0.6 MeV Bi ions [65]. As a first step toward resolution of this problem, the critical amorphization dose and annealing kinetics must be examined as a function of ion mass, ion energy, and crystal thickness.

## Acknowledgments

The authors thank the IVEM-Tandem Facility staff at Argonne National Laboratory for assistance during the ion irradiation work. The IVEM-Tandem Facility is supported as a user facility by the US DOE, Basic Energy Sciences, under contract W-31-10-ENG-38. Huijun Li, Michael Colella, and Mark Blackford provided assistance with the SEM and TEM work and

maintenance of the facilities at Ansto, and Ian Swainson assisted with the collection of neutron diffraction data at Chalk River. This work was supported in part by British Nuclear Fuels Limited (BNFL) and the Cambridge-MIT Institute. SR acknowledges NERC for financial support; grant number NER/I/S/2000/00920.

## References

[1] Heremans C, Weunsch B J, Stalick J K and Prince E 1995 *J. Solid State Chem.* **117** 108
[2] Vyaselev O, Arai K, Yamazaki J, Tagikawa M, Hanawa M and Hiroi Z 2003 *Physica* B **329** 959
[3] Raju N P, Dion M, Gingras M J P, Mason T E and Greedan J E 1999 *Phys. Rev.* B **59** 14489
[4] Harker A B 1988 *Radioactive Waste Forms for the Future* ed W Lutze and R C Ewing (Amsterdam: North-Holland) p 335
[5] Ball C J, Buykx W J, Dickson F J, Hawkins K, Levins D M, Smart R St C, Smith K L, Stevens G T, Watson K G, Weedon D and White T J 1989 *J. Am. Ceram. Soc.* **72** 404
[6] Dickson F J, Mitamura H and White T J 1989 *J. Am. Ceram. Soc.* **72** 1055
[7] Ewing R C, Weber W J and Clinard F W Jr 1995 *Prog. Nucl. Energy* **29** 63
[8] Stoll W 1998 *Mater. Res. Soc. Bull.* **23** 6
[9] Myers B R, Armantrout G A, Jantzen C M, Jostsons A, McKibben J M, Shaw H F, Strachan D M and Vienna J D 1998 *Technical Evaluation Panel Summary Report, Plutonium Immobilization Project, Report No.* UCRL-ID-129315
[10] Mariano A N 1989 *Geochemistry and Mineralogy of Rare Earth Elements, Reviews in Mineralogy* ed B R Lipin and G A McKay (Washington, DC: Mineralogical Society of America) p 309
[11] Wall F, Williams C T and Woolley A R 1999 *Mineral Deposits: Processes to Processing* vol 1, ed C J Stanley (Rotterdam: Balkema Publishers) p 687
[12] Williams C T, Wall F, Woolley A R and Phillipo S 1997 *J. Afr. Earth Sci.* **25** 137
[13] Lumpkin G R, Chakoumakos B C and Ewing R C 1986 *Am. Mineral.* **71** 569
[14] Lumpkin G R and Ewing R C 1992 *Am. Mineral.* **77** 179
[15] Lumpkin G R and Ewing R C 1995 *Am. Mineral.* **80** 732
[16] Lumpkin G R and Ewing R C 1996 *Am. Mineral.* **81** 1237
[17] Wall F, Williams C T, Woolley A R and Nasraoui M 1996 *Mineral. Mag.* **60** 731
[18] Gieré R, Buck E C, Guggenheim R, Mathys D, Reusser E and Marques J 2001 *Scientific Basis for Nuclear Waste Management XXIV* (*Materials Research Society Symposium Proceedings* vol 663) ed K P Hart and G R Lumpkin (Pittsburgh, PA: Materials Research Society) p 935
[19] Roberts S K, Bourcier W L and Shaw H F 2000 *Radiochim. Acta* **88** 539
[20] Hart K P, Zhang Y, Aly Z, Loi E, Stewart M W A, Brownscombe A, Ebbinghaus B and Bourcier W 2000 *Scientific Basis for Nuclear Waste Management XXIII* (*Materials Research Society Symposium Proceedings* vol 608) ed R W Smith and D W Shoesmith (Pittsburgh, PA: Materials Research Society) p 353
[21] Icenhower J P, McGrail B P, Schaef H T and Rodriquez E A 2000 *Scientific Basis for Nuclear Waste Management XXIII* (*Materials Research Society Symposium Proceedings* vol 608) ed R W Smith and D W Shoesmith (Pittsburgh, PA: Materials Research Society) p 373
[22] Zhang Y, Hart K P, Blackford M G, Thomas B S, Aly Z, Lumpkin G R, Stewart M W A, McGlinn P J and Brownscombe A 2001 *Scientific Basis for Nuclear Waste Management XXIV* (*Materials Research Society Symposium Proceedings* vol 663) ed K P Hart and G R Lumpkin (Pittsburgh, PA: Materials Research Society) p 325
[23] Zhang Y, Hart K P, Bourcier W L, Day R A, Colella M, Thomas B, Aly Z and Jostsons A 2001 *J. Nucl. Mater.* **289** 254
[24] Icenhower J P, Strachan D M, Lindberg M M, Rodriquez E A and Steele J L 2003 Dissolution kinetics of titanate-based ceramic waste forms: results from single-pass flow tests on radiation damaged specimens *Pacific Northwest National Laboratory Report No.* PNNL-14252
[25] Lumpkin G R 2001 *J. Nucl. Mater.* **289** 136
[26] Wald J W and Offermann P 1982 *Scientific Basis for Nuclear Waste Management V* ed W Lutze (New York: Elsevier) p 369
[27] Clinard F W Jr, Peterson D E, Rohr D L and Hobbs L W 1984 *J. Nucl. Mater.* **126** 245
[28] Weber W J, Wald J W and Matzke Hj 1986 *J. Nucl. Mater.* **138** 196
[29] Krivokoneva G K and Sidorenko G A 1971 *Geochem. Int.* **8** 113
[30] Lumpkin G R and Ewing R C 1988 *Phys. Chem. Min.* **16** 2
[31] Lumpkin G R, Hart K P, McGlinn P J, Payne T E, Gieré R and Williams C T 1994 *Radiochim. Acta* **66/67** 469

[32] Weber W J, Hess N J and Maupin G D 1992 *Nucl. Instrum. Methods Phys. Res.* B **65** 102
[33] Smith K L, Zaluzec N J and Lumpkin G R 1997 *J. Nucl. Mater.* **250** 36
[34] Wang S X, Wang L M, Ewing R C and Govindan Kutty K V 1999 *Microstructural Processes in Irradiated Materials* (*Materials Research Society Symposium Proceedings* vol 540) ed S J Zinkle, G E Lucas, R C Ewing and J S Williams (Pittsburgh, PA: Materials Research Society) p 355
[35] Wang S X, Wang L M, Ewing R C, Was G S and Lumpkin G R 1999 *Nucl. Instrum. Methods Phys. Res.* B **148** 704
[36] Wang S X, Begg B D, Wang L M, Ewing R C, Weber W J and Govindan Kutty K V 1999 *J. Mater. Res.* **14** 4470
[37] Wang S X, Wang L M and Ewing R C 2000 *J. Non-Cryst. Solids* **274** 238
[38] Lumpkin G R, Smith K L and Blackford M G 2001 *J. Nucl. Mater.* **289** 177
[39] Begg B D, Hess N J, McCready D E, Thevuthasan S and Weber W J 2001 *J. Nucl. Mater.* **289** 188
[40] Meldrum A, White C W, Keppens V, Boatner L A and Ewing R C 2001 *Phys. Rev.* B **63** 104109
[41] Lian J, Zu X T, Govindan Kutty K V, Chen J, Wang L M and Ewing R C 2002 *Phys. Rev.* B **66** 054108
[42] Stewart M W A, Begg B D, Vance E R, Finnie K, Li H, Lumpkin G R, Smith K L, Weber W J and Thevuthasan S 2002 *Scientific Basis for Nuclear Waste Management XXV* (*Materials Research Society Symposium Proceedings* vol 713) ed B P McGrail and G A Cragnolino (Pittsburgh, PA: Materials Research Society) p 311
[43] Lian J, Wang L M, Haire R G, Helean K B and Ewing R C 2004 *Nucl. Instrum. Methods Phys. Res.* B **218** 236
[44] Lumpkin G R, Smith K L, Blackford M G, Gieré R and Williams C T 1994 *Micron* **25** 581
[45] Allen C W, Funk L F and Ryan E A 1996 *Mater. Res. Soc. Proc.* **396** 641
[46] Chakoumakos B C 1984 *J. Solid State Chem.* **53** 120
[47] Shannon R D 1976 *Acta Crystallogr.* A **32** 751
[48] Subramanian M A, Aravamudan G and Subba Rao G V 1983 *Prog. Solid State Chem.* **15** 55
[49] Tabira Y, Withers R L, Yamada T and Ishizawa N 2001 *Z. Kristallogr.* **216** 92
[50] Weber W J 2000 *Nucl. Instrum. Methods Phys. Res.* B **166/167** 98
[51] Jiang W, Weber W J, Thevuthasan S and Sutthanandan V 2001 *J. Nucl. Mater.* **289** 96
[52] Zinkle S J and Kinoshita C 1997 *J. Nucl. Mater.* **251** 200
[53] Cooper R, Smith K L, Colella M, Vance E R and Philips M 2001 *J. Nucl. Mater.* **289** 199
[54] Smith K L, Colella M, Cooper R and Vance E R 2003 *J. Nucl. Mater.* **321** 19
[55] Veiller L, Crocombette J-P and Ghaleb D 2002 *J. Nucl. Mater.* **306** 61
[56] Chartier A, Meis C, Crocombette J-P, Corrales L R and Weber W J 2003 *Phys. Rev.* B **67** 174102
[57] Lian J, Chen J, Wang L M, Ewing R C, Farmer J M, Boatner L A and Helean K B 2003 *Phys. Rev.* B **68** 134107
[58] Lian J, Ewing R C, Wang L M and Helean K B 2004 *J. Mater. Res.* **19** 1570
[59] Ewing R C, Lian J and Wang L M 2004 *Mater. Res. Soc. Proc.* **792** 37
[60] Kennedy B J, Hunter B A and Howard C J 1997 *J. Solid State Chem.* **130** 58
[61] Meldrum A, White C W, Keppens V, Boatner L A and Ewing R C 2001 *Phys. Rev.* B **63** 104109
[62] Wang S X, Wang L M and Ewing R C 2000 *J. Non-Cryst. Solids* **274** 238
[63] Sickafus K E, Minervini L, Grimes R W, Valdez J A, Ishimaru M, Li F, McClellan K J and Hartmann T 2000 *Science* **289** 748
[64] Minervini L and Grimes R W 2000 *J. Am. Ceram. Soc.* **83** 1873
[65] Begg B D, Hess N J, Weber W J, Devanathan R, Icenhower J P, Thevuthasan S and McGrail B P 2001 *J. Nucl. Mater.* **288** 208